Authors' final version of a paper published in "Neurocomputing"

Paper reference:
Y. Deville, J. Damour, N. Charkani, "Multi-tag radio-frequency identification systems based on new blind source separation neural networks", Neurocomputing, vol. 49, pp. 369-388, 2002.

Multi-tag radio-frequency identification systems based on new blind source separation neural networks

Yannick DEVILLE[(1)], Jacques DAMOUR[(2)], Nabil CHARKANI[(3)]

[(1)] Laboratoire d'Acoustique, de Métrologie, d'Instrumentation,
Bât. 3R1B2, 118 Route de Narbonne, 31062 Toulouse Cedex, France.
[(2)] Laboratoires d'Electronique Philips S.A.S, 22 Avenue Descartes, B.P. 15,
94453 Limeil-Brévannes Cedex, France.
[(3)] Philips Consumer Communications, Advanced Development,
177-181 Av. Pierre Brossolette, 92120 Montrouge, France.

Corresponding author: Yannick DEVILLE. Postal address: see [(1)] above. E-mail address: ydeville@cict.fr . Fax number: + 33 5 61 55 81 54.
Keywords: artificial neural network, blind source separation, identification system, radio-frequency communication, self-normalized algorithm.
Abstract: Electronic systems are progressively replacing mechanical devices or human operation for identifying people or objects in everyday-life applications. Especially, the radio-frequency contactless identification systems available today have several advantages, but they cannot handle easily several simultaneously present items. This paper describes a solution to this problem, based on blind source separation techniques. The effectiveness of this approach is experimentally demonstrated, using workstation and real-time DSP-based implementations of the proposed system. More precisely, various source separation neural networks are compared, and the networks that we proposed recently are shown to be the most attractive ones, thanks to their simplicity, good performance and self-normalized (i.e. "automated") operation.

1 Introduction

Many real-world situations require to identify people, animals or objects. Typical examples are owner identification before starting car engines, access control for restricted areas, cattle identification or control of the flow of manufactured products in factories. In the past, the approaches used to perform such identifications were mainly based on mechanical devices (such as keys for starting car engines), or human operation (e.g. visual inspection of people, cattle or products in the above examples). These approaches are progressively being replaced by various types of electronic systems, and especially by systems based on radio-frequency (RF) communication.

Such an RF system [10],[19],[20],[22] is shown in Fig. 1. It consists of a base station inductively coupled to portable identifiers (called "tags") which contain an LC resonator, a controller and non-volatile programmable memory (EEPROM). The memory contents are specific to each tag and allow to identify the tag-bearer (person or object). The basic mode of operation of this system may be modelled as follows. The base station emits an RF sine wave, which is received by a single tag. The tag is thus powered and answers by emitting a sine wave at the same frequency (due to inductive coupling), modulated by its encoded memory contents. The base station receives this signal, demodulates it, and decodes it so as to determine the memory contents (details of the coding scheme are

presented in Appendix B). The overall identification system then checks these data and controls its actuators accordingly.

This type of system is attractive because it yields contactless operation between the base station and tags (thus avoiding constraints on the positions of the tag-bearers), and because it operates with battery-less tags. However, when two tags are placed in the RF field of the base station, both tags answer this station. The demodulated signal derived by this station is then a mixture of two components, and cannot be decoded by this basic station. This system is therefore unable to identify two simultaneously present tag-bearers. A few attempts to solve this type of problem have been presented in the literature. Some consist in making the base station and tags communicate according to a predefined protocol, so that each tag successively provides its contents [4]. This approach entails slow operation and yields a complex system, since significant circuitry must be added to the base station and tags in order to implement the communication protocol. This solution is therefore not attractive. Another approach consists in using tags which operate at different frequencies [12]. This again yields complex circuitry and requires a large frequency band to be allocated to the system, which is not always possible. The approach presented in this paper aims at avoiding all these drawbacks. This is achieved by resorting to blind source separation techniques, which form an emerging area in the fields of artificial neural networks and signal processing.

The remainder of this paper is organized as follows. The overall structure of the proposed system is presented in Section 2. Alternative approaches for its source separation unit are depicted in Section 3, including classical neural networks and extensions that we recently proposed. The experimental performance of all resulting versions of this system is reported in Section 4. Conclusions are drawn in Section 5 and specific topics are developed in the appendices.

2 Overall proposed system

The system proposed in this paper (Fig. 2) for simultaneously handling two tag signals is an extension of the standard system described above. It relies on a base station containing two reception antennas and two demodulators, which yield two mixed signals. These mixed signals are processed by a blind source separation unit, which extracts the two components corresponding to the two tags. Then, by decoding these separated signals, the memory contents of the two tags are obtained independently.

More precisely, the nature of the available mixtures of signals is derived from the theoretical analysis provided in Appendix A of this paper and confirmed by the experimental tests reported in Subsection 4.2. This shows that the modulation/demodulation scheme used in this system is such that the mixed signals provided by the demodulators are restricted to their simplest possible form, i.e. they are linear instantaneous mixtures (as defined in Section 3) of the components corresponding to the two tags. Many source separation approaches suited to such mixtures have been proposed in the last 15 years. A survey of this field may be found e.g. in [1]. In the current paper, we use a class of available approaches inspired from the field of artificial neural networks, and we investigate their performance when applied to the proposed system. We also consider modified versions of this type of approaches that we recently introduced, and we benchmark them against the classical solutions. All these approaches are described in Section 3. They were selected in this investigation for the following reasons. First, their convergence properties are well defined in the considered two-source configuration and they are such that these

approaches do apply to the type of sources considered in this application, as will be shown in the subsequent sections of this paper. In addition, these approaches are based on adaptive algorithms, which makes them able to track easily evolving mixtures which occur in our application when tag-bearers are moving. Finally, they use very simple computations, which makes them particularly attractive for the final low-cost real-time implementation targetted in this investigation.

It should be noted that the system thus obtained meets the requirements defined in Section 1: 1) it yields fast operation by allowing two tags to communicate simultaneously with the base station; 2) all the tags have the same simple structure as in the standard single-tag system, and the added complexity only appears in the base station, i.e. in a single location of the system, so that its cost is limited; 3) the system uses a single carrier frequency.

3 Blind source separation problem and solutions

In the "simplest configuration" of the blind source separation problem, two signals $E_1(t)$ and $E_2(t)$ are available, and these signals are unknown linear instantaneous mixtures of two unknown supposedly statistically independent source signals $X_1(t)$ and $X_2(t)$, i.e:

$$E_1(t) = a_{11}X_1(t) + a_{12}X_2(t) \tag{1}$$

$$E_2(t) = a_{21}X_1(t) + a_{22}X_2(t), \tag{2}$$

where the terms a_{ij} are unknown real-valued mixture coefficients. Blind source separation then consists in estimating the source signals $X_j(t)$ from the mixed signals $E_i(t)$ up to an arbitrary permutation and an arbitrary scale factor. As explained above, this generic problem is faced in the system considered in this paper, where the mixed signals are the demodulator outputs, whereas the sources to be restored are the encoded tag memory contents. The remainder of this section describes all the solutions to this generic problem which are considered in this paper. This includes three related neural approaches available from the literature and two original solutions that we recently introduced.

The first classical approach, proposed by Hérault and Jutten (see esp. [14],[15]), is based on the recurrent artificial neural network shown in Fig. 3 in the case of the above-defined "simplest configuration". c_{12} and c_{21} are the adaptive weights of this neural network[1]. They are updated according to the following nonlinear unsupervised learning rule:

$$c_{ij}(n+1) = c_{ij}(n) - af[s_i(n)]g[s_j(n)], \tag{3}$$

where a is a positive adaptation (or learning) gain, $s_i(t)$ and $s_j(t)$ are the (estimated) centered versions of the network outputs $S_i(t)$ and $S_j(t)$, and f and g are typically odd functions.

The functions f and g have a major influence on the type of sources that this network can separate. Their selection is therefore of utmost importance in practical applications such as the one described in this paper, and may be performed as follows. When arbitrary odd nonlinear functions f and g are used, the network is only able to separate (some types of) symmetric sources [6]. As shown in [6], this restriction may be avoided by using either

[1] As compared to the original papers by Hérault and Jutten, the signs of the weights c_{12} and c_{21} have been changed in Fig. 3, in order to be homogeneous with the subsequent figures of the current paper. The rule (3) used to update these weights has been modified accordingly.

$f = (.)$ or $g = (.)$ (and not both because this would result in using only the second-order statistics of the signals and it would not guarantee that this algorithm reaches separation [15]). Especially, two sets of functions are attractive, due to their simplicity and to the type of sources to which they apply, i.e:

$$f = (.)^3 \quad \text{and } g = (.), \tag{4}$$

and

$$f = (.) \quad \text{and } g = (.)^3. \tag{5}$$

The choice between these two sets of functions is to be made depending on the considered type of sources (to ensure that the network weights converge to values which yield separated signals at the network outputs): (4) applies to globally sub-Gaussian sources [5],[11],[17],[18],[21] i.e. to sources such that $R < 9$, where R is the ratio defined as:

$$R = \frac{E\{x_1^4\}E\{x_2^4\}}{(E\{x_1^2\})^2(E\{x_2^2\})^2}, \tag{6}$$

and where $x_j(t)$ are the centered versions of the sources $X_j(t)$ and $E\{\}$ stands for mathematical expectation. It may be shown[2] that (5) applies to globally super-Gaussian sources, i.e. to sources such that $R > 9$.

In the system considered in this paper, the sources are expected to be globally sub-Gaussian, as shown by the theoretical analysis provided in Appendix B. Therefore, the version of the above-defined network which should be able to separate these signals is the one corresponding to (4). This is confirmed experimentally in Section 4.

Moreau and Macchi [16],[17],[18] proposed a direct (i.e. non-recurrent) version of the Hérault-Jutten network (see Fig. 4), adapted with the same rule (3) as the latter network. They also studied the convergence properties of this network in the "simplest configuration". They especially showed that, for this network too, the functions defined in (4) allow to separate sub-Gaussian signals.

Cichocki et al. [2] also defined neural networks which may be considered as extensions of the above ones. These extended networks contain additional self-adaptive weights, which are updated so as to normalize the "scales" of the network outputs. Both the direct and recurrent versions of this type of neural networks were described, and it was also proposed to cascade them in a multilayer neural network in order to improve performance. In this paper, we only consider the direct version of these networks, as it yields the same feature as the Moreau-Macchi network as compared to the corresponding recurrent structure. Moreover, we focus ourselves on the single-layer version of this network. We showed elsewhere [7] that, for this network too, the functions defined in (4) allow to separate sub-Gaussian signals.

We here also use another type of self-normalized source separation neural networks, that we recently introduced. Their principles and features are detailed in [9] and summarized hereafter. This type of networks is based on the same structures as the above-mentioned classical approaches: they may contain one or several layers, and each layer may have a recurrent or a direct form. The single-layer versions of these networks are resp. shown in Fig. 3 and 4 for the case of 2 source signals, and are extended to a higher number of sources in the same way as for the Hérault-Jutten and Moreau-Macchi networks. The

[2]This may be shown e.g. by adapting the approach of [21] to the functions defined in (5).

proposed networks differ from the previous ones in the algorithm used to update their weights, which here reads:

$$c_{ij}(n+1) = c_{ij}(n) - a\frac{f[s_i(n)]}{\sqrt{E[f^2(s_i)]}}\ \frac{g[s_j(n)]}{\sqrt{E[g^2(s_j)]}}. \tag{7}$$

The normalizing terms $\sqrt{E[f^2(s_i)]}$ and $\sqrt{E[g^2(s_j)]}$ that we introduced in this rule, as compared to the classical rule (3), are estimated in practical situations, using first-order low-pass filtering. When the functions f and g are set to (4), the adaptation rule (7) becomes:

$$c_{ij}(n+1) = c_{ij}(n) = -a\frac{s_i^3(n)}{\sqrt{E[s_i^6]}}\ \frac{s_j(n)}{\sqrt{E[s_j^2]}}. \tag{8}$$

When a scale factor λ is applied to both mixed signals (and therefore to $s_i(t)$ and $s_j(t)$), the right-hand term of (8) remains unchanged, thanks to the normalizing terms that we introduced. The weight trajectories achieved by this rule, and hence its convergence speed and accuracy, are therefore completely insensitive to the common "level" of the signals, which is an attractive feature because this level is unknown in practice. These convergence speed and accuracy are then controlled by the selected adaptation gain a: a low gain yields good convergence accuracy at the expense of low convergence speed, whereas a high gain yields opposite features, so that the selection of the adaptation gain value makes it possible to achieve the desired convergence speed/accuracy trade-off. On the contrary, the classical Hérault-Jutten and Moreau-Macchi networks do not yield such a controlled convergence speed/accuracy trade-off. This is our main motivation for considering the proposed self-normalized rule here. This rule has several other attractive features, most of which hold for any functions f and g. A complete description of these properties is beyond the scope of this paper, but several of them may be found in [9]. Especially, these self-normalized networks lead to the same type of considerations as above about the functions f and g to be selected, e.g. among (4) and (5), depending on the type of sources to be processed (see details in [9]).

4 Experimental results

4.1 Experimental setup

The experimental setup used for checking the effectiveness of the proposed approach is represented in Figure 5. The antennas and tags each consist of a horizontal disk (with a diameter of 52 mm for the antennas and 28 mm for the tags). The tags lie on a horizontal plastic plane, whereas the antennas correspond to horizontal planes resp. situated at distances h_1 and h_2 below the tag plane. As explained above, the tags, antennas and demodulators used in these experiments are those of the standard commercial system available when performing this investigation. The emission/reception range of this system is limited, i.e. each tag should be at a distance lower than 60 mm from a base station to be detected. In the considered setup, this required us to put the tags close to the antennas i.e: $h_1 = 35$ mm and $h_2 = 25$ mm. The distance D between the tags was varied in the experiments. When the tags are close one to the other (i.e. D similar to the tag diameter), the standard system fails to identify the tags, so that the source separation unit presented

in this paper is required. This is the configuration considered in the remainder of this paper.

It should be noted that the dimensions of this setup are relevant for various real-world applications, such as car immobilization. In this case, the tag is located in a classical mechanical key and its contents are checked when the car owner starts the engine. The multi-tag situation then arises when one or several other electronic keys corresponding to other applications (e.g. to another car) are hooked together with the key of the considered car, so that the signal emitted by the latter key is disturbed by the signals emitted by the other keys. In such a case, the standard single-antenna base station is unable to identify the contents of the key corresponding to that car, so that the multiple-antenna system introduced in this paper is required. Some applications (such as the ones listed in Section 1) involve dimensions which are significantly higher than those in the setup used in this paper. For such applications, this setup should be considered as a preliminary down-scaled version of the target system. The real system will then be derived from this setup by using longer-range emission/reception units.

4.2 Experimental nature of the sources and mixtures

The first experiments performed with the above-defined setup aimed at checking that the sources and mixtures encountered in this setup actually have the nature derived from the theoretical analyses mentioned in the previous sections of this paper.

A first set of experimental measurements showed that, for each of the considered source signals $x_j(t)$, the ratio $E\{x_j^4\}/(E\{x_j^2\})^2$ is close to 1.3. Therefore, the parameter R defined in (6) is close to 1.7 for each couple of such sources. This confirms that the actual sources are strongly globally sub-Gaussian. All the source separation experiments reported in the next subsections were therefore performed with neural networks operating with the functions defined in (4).

We then checked the experimental nature of the mixtures. As a first step, we verified that these mixtures are instantaneous. To this end, we successively used two methods. We first made a qualitative verification, by placing a single tag in the RF field of our two-antenna base station, and displaying the outputs of both demodulators on an oscilloscope. These two signals were thus observed to be proportional with no time delay, which corresponds to instantaneous mixtures (see (1)-(2): the two signals corresponding e.g. to tag 1 are: $a_{11}X_1(t)$ and $a_{21}X_1(t)$). This result was then confirmed by using a quantitative method: with the same configuration (i.e. one tag in the RF field of our two-antenna base station), we sampled the outputs of both demodulators at 32 kHz[3]. We then analyzed the sequence of cross-correlation coefficients of these two signals, i.e:

$$\rho(\tau) = \frac{E\{s_1(t)s_2(t+\tau)\}}{\sqrt{E\{s_1^2(t)\}}\sqrt{E\{s_2^2(t)\}}}. \tag{9}$$

The complete cross-correlation sequence thus obtained with signals consisting of 8000 samples is represented in Figure 6 (a). The periodic nature of this cross-correlation sequence results from the fact that the considered signals are themselves periodic, since they consist of a succession of identical frames containing about 2000 samples (see Appendix B). A zoom of this cross-correlation sequence around lag zero is shown in Figure 6 (b). This

[3]This frequency was used because it was the only one available in the considered setup. However, a lower frequency is presumably acceptable for the signals to be processed here.

shows that the cross-correlation coefficient $\rho(\tau)$ reaches its maximum exactly for $\tau = 0$, and that this maximum is very close to 1. The two considered signals are therefore proportional with no time delay, which confirms the instantaneous nature of the mixtures.

The second step of our investigation of the experimental nature of the mixtures aimed at checking the linearity of these mixtures. The main origins of non-linear behaviour in the considered system are presumably the demodulators, while the superposition of the signals received by the antennas is expected to be linear. Therefore, we only analyzed the linearity of the demodulators. To this end, we applied a carrier signal modulated by a sine wave at the input of a demodulator. We varied the magnitude of the modulating sine wave and we studied the resulting variations of the magnitude of the output of the demodulator. These variations are represented in Figure 7. The demodulator was thus shown to have a linear behaviour for a modulation magnitude up to about 1.5 V. This defined the minimum tag-antenna distance required for ensuring linear operation, i.e. about 1 cm. That is why the tags were placed on a plane situated a few centimeters above the antennas in the considered setup, as stated above.

All the investigations described in this subsection showed that the source signals and mixtures involved in the considered setup indeed have the properties required by the considered neural networks. Since these requirements were met, we then proceeded to experiments focused on the performance of the system from the point of view of the separation of these source signals.

4.3 Separation from artificial mixtures

The first set of source separation experiments was performed with artificial mixtures of real sources, successively applied to each one of the five types of neural networks defined in Section 3, i.e:

- the Hérault-Jutten network,
- the Moreau-Macchi network,
- the single-layer direct Cichocki network,
- the two single-layer versions of the networks that we proposed, resp. based on a recurrent and a direct structure, and resp. denoted NWUr and NWUd below (where "NWU" refers to the Normalized Weight Updating algorithm used in these networks).

The goal of these experiments was twofold. On the one hand, they aimed at checking that all these networks can actually separate the source signals which occur in the real considered system, assuming these signals are mixed in a linear instantaneous way. On the other hand, they allowed us to compare the performance of all these networks in various situations and to select the best networks.

More precisely, these experiments were performed in the following conditions. In order to create artificial linear instantaneous mixtures of real source signals, a single tag was first placed in the RF field of the base station. The resulting output of one of the demodulators of the base station was sampled, thus providing a single source signal $X_1(t)$. This tag was then removed and a second tag was placed in the RF field of the base station. The same measurement procedure as above was carried out for this second tag, thus providing another source signal $X_2(t)$. Two artificial mixtures $E_1(t)$ and $E_2(t)$ of these two sources

were then computed according to (1)-(2). These mixed signals were then provided to software implementations of the considered networks operating with floating-point numbers on a workstation. Two cases were successively considered for the values of the mixture coefficients a_{ij}. In both cases, a_{11} and a_{22} were set to 1. The complexity of the considered mixture was then defined by the values of a_{12} and a_{21}, which were selected as follows:

- The first experiments were performed with $a_{12} = 0.4$ and $a_{21} = 0.3$. These values correspond to a medium mixture ratio, and are similar to the actual values in the experimental setup defined above (as may be derived from the results provided in Subsection 4.4).
- The other experiments were performed with $a_{12} = a_{21} = 0.98$. This corresponds to a very high mixture ratio, which may esp. occur in long-range systems when two tags are very close one to the other as compared to the tag-antenna distances. The sources are then expected to be quite hard to separate, since the two mixed signals $E_1(t)$ and $E_2(t)$ provided to the networks are very similar, as can be seen by applying these values of the mixture coefficients a_{ij} to (1)-(2).

The performance achieved in each experiment is defined by the two parameters considered in Section 3, i.e. the convergence speed and accuracy of the selected network. The convergence speed is measured by the number of samples required for all network weights to have converged to their equilibrium values, which is called the "convergence time" and denoted T_c below[4]. The convergence accuracy is measured by the Signal to Noise Ratio Improvement ($SNRI$) provided by the network. This parameter, which takes large values when the network restores well separated sources, is defined by: $SNRI = (SNRI_1 + SNRI_2)/2$. Each term $SNRI_i$ of this expression denotes the Signal to Noise Ratio Improvement provided by output i of the network with respect to source i, expressed in dB. For the Hérault-Jutten and NWUr networks, when source separation without a permutation is achieved exactly, $S_i(t)$ becomes equal to $a_{ii}X_i(t)$ [8],[15]. For these networks, $SNRI_i$ is therefore defined by:

$$SNRI_i = 10log_{10}\left[\frac{E\{(E_i(t) - a_{ii}X_i(t))^2\}}{E\{(S_i(t) - a_{ii}X_i(t))^2\}}\right]. \tag{10}$$

Similarly, the Moreau-Macchi and NWUd networks yield:

$$SNRI_i = 10log_{10}\left[\left(\frac{a_{11}a_{22} - a_{12}a_{21}}{a_{11}a_{22}}\right)^2 \cdot \frac{E\{(E_i(t) - a_{ii}X_i(t))^2\}}{E\left\{\left(S_i(t) - \frac{(a_{11}a_{22} - a_{12}a_{21})X_i(t)}{a_{jj}}\right)^2\right\}}\right], \tag{11}$$

whereas the direct Cichocki network leads to:

$$SNRI_i = 10log_{10}\left[\frac{1}{a_{ii}^2 E\{x_i^4(t)\}^{\frac{1}{2}}} \cdot \frac{E\{(E_i(t) - a_{ii}X_i(t))^2\}}{E\left\{\left(S_i(t) - \frac{X_i(t)}{E\{x_i^4(t)\}^{\frac{1}{4}}}\right)^2\right\}}\right]. \tag{12}$$

[4]These convergence times were estimated from the plots representing the evolution of the network weights vs time.

As explained in Section 3, the overall performance of a given network is defined by the trade-off between T_c and $SNRI$ achieved by this network. This trade-off was determined by performing experiments for various values of the network adaptation gain a, recording the values of T_c and $SNRI$ obtained in these conditions and plotting the resulting variations of $SNRI$ vs T_c. The results thus obtained are shown in Fig. 8 and 9, resp. for the two considered sets of mixture coefficients. The part of main interest in these figures is the one corresponding to the range of values of T_c required in practical applications, which may be defined as follows. As explained above, the data received from a tag by the base station of a standard single-tag system consists of a series of identical frames, which contain about 2000 samples. Moreover, when the tag enters the field of the base station and progressively starts emitting, the base station has to wait until it receives a clean synchronization sequence (situated at the beginning of a frame) before it can start decoding the received signal. In other words, the base station has an intrinsic latency period of typically one frame. Therefore, in a multi-tag system, one would like the source separation network to converge during this latency period, so that it would then provide separated sources from the first completely clean received frame. Thus, adding such a network to the original single-tag identification system in order to achieve multi-tag capability would not slow this system down. A typical target value for T_c is therefore about one frame, or 2000 samples. Moreover, various applications can accept somewhat higher response times (i.e. typically a few frames), as the duration of a single frame is only about 70 ms, which is quite low as compared to the response times actually required from a user point of view in many identification applications. Therefore, a selection among the considered networks is made hereafter by taking into account their performance not only around $T_c = 2000$ samples, but also in a range typically covering $T_c = 2000$ to 10000 samples (i.e. up to 5 frames).

Fig. 8 and 9 first show that the Moreau-Macchi network should preferably not be used in the considered application, as it cannot achieve the desired T_c for high mixture ratios. The Cichocki network is not attractive either because: i) it cannot reach $T_c \simeq 2000$ samples (or its $SNRI$ is then rather low) and ii) for any T_c in the considered range, its $SNRI$ is lower than or equal to that of the remaining three networks, i.e. Hérault-Jutten, NWUr and NWUd. Among the latter three networks, the preferred ones depend as follows on the main parameter of interest in the considered application. All three networks can reach $T_c \simeq 2000$ samples (with an acceptable $SNRI$), but this is almost the limit achievable by the NWUd network. Therefore, if minimizing T_c is of utmost importance in the considered application, the HJ and NWUr networks should be preferred. On the contrary, if the emphasis is laid on the performance of the network for high mixture ratios, while the value of T_c (within the considered range) is not critical, NWUd should be preferred.

Up to this point, we only considered the performance (in terms of T_c and $SNRI$) of the considered networks. But, as explained in Section 3, another feature of these networks should also be taken into account, i.e. their ability to operate in a self-normalized (or "automated") way, i.e. without depending on signal levels. Then, in addition to the Moreau-Macchi and Cichocki networks, the Hérault-Jutten network is also rejected. In other words, the preferred networks in the considered application are NWUr and NWUd (and the eventual selection between these two networks depends whether the emphasis is laid on a low T_c or on high mixture ratios, as explained above). Therefore, only these two networks are considered hereafter. Moreover, their adaptation gain a is set to the value which yields $T_c \simeq 2000$ samples in the experiments with similar mixture coefficients reported above, i.e: $a = 10^{-3}$ for both networks.

4.4 Separation from real mixtures

The second set of source separation experiments was performed with the actual system. To this end, two tags were placed simultaneously in the RF field of the base station, and the resulting mixed output signals $E_1(t)$ and $E_2(t)$ of the two demodulators were measured. These two real mixed signals were then used as the inputs of the software NWUr or NWUd network. Figure 10 shows the evolution of the weights thus obtained for the NWUr network, when its learning gain is set to $a = 10^{-3}$. This gain value yields $T_c \simeq 2000$ samples, which is completely coherent with the results obtained with artificial mixtures in Subsection 4.3. The experiments performed with the NWUd network lead to the same results.

Figure 10 also shows that the network weights converge towards different values. This results from the fact that the values of the network weights for which source separation is achieved depend on the values of the mixture coefficients [8], which are here different due to the physical asymmetry of the setup (see Fig. 5). As these mixture coefficients are unknown here, the theoretical network weight values corresponding to source separation and the experimental $SNRI$ (10)-(11) cannot be computed. Another approach should therefore be used to check if the networks succeed in restoring the source signals. The alternative method used here consists in providing the network outputs to the decoders of the system. As explained above, these decoders wait for the first synchronization sequence in the network outputs, and then provide the restored tag data. Comparing these data with the original data stored in the tags[5] here shows that they are exactly the same. In other words: 1) the NWUr and NWUd neural networks do not slow down the system, because they converge in a period of about one frame, during which the decoders have to wait for a synchronization sequence anyway, and 2) after convergence they provide a perfect restoration of the sources from an application point of view, in the sense that they restore the bitstreams of the tags without any errors.

4.5 Real-time implementation

Based on the success of the experiments reported above, we developed a real-time implementation of some of the above approaches, using a DSP board which operates only with fixed-point numbers. Extensive tests showed that the resulting real-time system converges at almost the same speed as the floating-point version and that the tag data are decoded exactly after convergence. These tests also demonstrated the long-term stability of the considered networks. Moreover, they allowed us to check the ability of these networks to track varying mixtures.

5 Discussion and conclusions

The investigations presented in this paper demonstrate that blind source separation neural networks make it possible to achieve multi-tag capability with limited means in identification systems. More precisely, among all the source separation methods that we compared, the new approaches that we proposed were shown to be the most attractive ones, thanks to their simplicity, good performance and self-normalized (i.e. "automated") operation.

[5] Of course, the data stored in the tags are only known in the tests considered here, whereas they are unknown during the real operation of the system, when the identification of these data is to be performed.

The possible extensions of this investigation deserve the following comments. In the configuration considered above, the proposed approaches are particularly attractive, as they meet the requirements set by the application with very low computational complexity, whereas most other approaches are likely to yield more complex implementations. Some of the approaches available in the literature might become of interest in two other types of configurations however, i.e:

- in future applications of identification systems which may require lower response times and should then include source separation units which can converge more quickly,
- and in applications involving more than two tags. Extended versions of the approaches considered in this paper may be defined easily for the case when more than two sources are to be separated. However, their convergence properties are less clearly defined at this stage. An alternative may then consist in using some approaches of the literature which have been shown to have guaranteed convergence. This esp. includes the approach based on kurtosis introduced in [3], which was subsequently extended in various ways such as in [13].

  It should be remembered anyway that various identification systems have a limited emission/reception range. In such systems, only the tags which are quite close to the base station yield non-negligible signals. This inherently limits the number of tags to be considered to a small number, possibly down to two e.g. if the physical structure of the system restricts the number of tags that may be close to the base station. A large range of identification applications are therefore covered by the configuration and solution considered in this paper.

Another possible extension of this investigation concerns the use of source separation for reducing background RF noise, thus allowing i) higher distances between the base station and tags, or ii) lower power consumption. Also, the available *a priori* knowledge about the sources was only partly used in the approaches considered up to now. This allowed us to develop a versatile approach, which may be extended to other (identification) systems. However, a fine-tuned approach dedicated to the specific system considered in this paper may also be developed, by using a source separation unit which would take more advantage of this knowledge about the sources to be processed.

Acknowledgements

The authors would like to thank Laurence Andry for her support during the first stages of this activity and the anonymous reviewers for their comments.

A Theoretical nature of the mixtures

This appendix demonstrates that, in an ideal model of the system described in Section 2, the mixed signals to be processed by the source separation unit are linear instantaneous mixtures of the components corresponding to the two tags. As shown below, this nature of the mixtures results from the modulation/demodulation scheme used in this system, i.e. a low-frequency amplitude modulation.

To prove this result, let us consider the successive steps of the propagation and processing of the considered signals. Initially, a carrier signal $Vsin\omega t$ is emitted by the base station. It is received by each tag j with a delay τ_j and a multiplying coefficient α_j (related to the attenuation of this signal which occurs during propagation). The signal received by tag j at time t is thus: $\alpha_j V sin[\omega(t-\tau_j)]$. Assuming that this tag performs an ideal amplitude modulation of this carrier by its encoded tag data signal $x_j(t)$, the signal emitted by tag j at time t is: $x_j(t)\alpha_j V sin[\omega(t-\tau_j)]$.

Now consider one of the reception antennas of the base station (the same principle applies to each of these antennas). It receives each emitted tag signal with a delay τ'_j and a multiplying coefficient α'_j. Each tag signal received by this antenna at time t is thus: $a_j x_j(t-\tau'_j)Vsin[\omega(t-\tau_j-\tau'_j)]$, with: $a_j = \alpha_j\alpha'_j$. This antenna ideally performs a linear superposition of the contributions received from the two tags. The overall signal received by this antenna at time t is thus:

$$a_1 x_1(t-\tau'_1)Vsin[\omega(t-\tau_1-\tau'_1)] + a_2 x_2(t-\tau'_2)Vsin[\omega(t-\tau_2-\tau'_2)]. \qquad (13)$$

This overall received signal may be rewritten as:

$$\begin{aligned} &sin\omega t[a_1 V x_1(t-\tau'_1)cos\phi_1 + a_2 V x_2(t-\tau'_2)cos\phi_2] \\ &+cos\omega t[a_1 V x_1(t-\tau'_1)sin\phi_1 + a_2 V x_2(t-\tau'_2)sin\phi_2] \end{aligned} \qquad (14)$$

with: $\phi_j = -\omega(\tau_j+\tau'_j) = -2\pi f L_j/c$, where f is the carrier frequency, L_j is the overall propagation distance (i.e. from the emitting antenna to tag j and then back to the reception antenna) and with: $\tau'_j = l'_j/c$, where l'_j is the propagation distance from the tag to the reception antenna only.

In the considered system, these parameters have the following typical numerical values: $f = 125\ kHz$ and $L_j < 10\ cm$, so that $|\phi_j| < 2.6 * 10^{-4} \ll 1$; in addition, $l'_j < 5\ cm$, so that $\tau'_j < 1.7 * 10^{-10} s \ll T \simeq 10^{-3} s$, where T is the period of the modulating signal. Due to these values, the overall signal received by an antenna may be approximated by: $sin\omega t[a_1 V x_1(t) + a_2 V x_2(t)]$. The resulting output of an ideal amplitude demodulator is therefore: $a_1 V x_1(t) + a_2 V x_2(t)$. This signal, which is provided to the source separation unit is thus indeed a linear instantaneous mixture (as defined in Section 3) of the modulating signals $x_1(t)$ and $x_2(t)$ of the two tags. It should be noted that this result also applies to the case when each tag signal propagates through several paths to the base station: each path then yields an individual contribution; however, when neglecting all propagation delays as explained above, all these contributions are merged into a single overall signal which follows the above model.

B Theoretical nature of the sources

In this appendix, we present a model of the sources encountered in the system under investigation, which are to be restored by the source separation unit of this system. Each such source consists of a succession of identical frames. Each frame contains a synchronization sequence followed by data (i.e. the tag memory contents). Moreover, these data are encoded by using a standard coded diphase procedure, which is defined hereafter.

As a first step, let us consider only the ideal operation of the system for encoded data (i.e. excluding synchronization sequences). Ideally, each data bit equal to 0 is encoded as a voltage equal to a value $+V$ during half a cycle, followed by the opposite voltage $-V$ during the other half of the cycle. The bits equal to 1 are encoded by alternating values,

i.e. a voltage equal to $+V$ during a complete cycle for one bit equal to 1, and a voltage equal to $-V$ during a complete cycle for the next bit equal to 1. This ideal signal may be represented as a random stationary source, taking the values -1 and 1 (in units defined by the voltage $+V$) with a probability 1/2, whatever the values of the bits that it encodes. As a result, the couple of sources to be separated may be shown to be such that $R = 1$, where R is defined in (6). It is therefore such that R is much lower than the threshold value $R = 9$, i.e. it is strongly globally sub-Gaussian (see Section 3).

In the real identification system, the source signals are significantly distorted and are therefore not binary valued. In addition, they contain synchronization sequences which are not symmetric. The corresponding ratio R may therefore be somewhat different from its theoretical value $R = 1$, but is expected to remain significantly lower than the threshold value $R = 9$. In other words, the real sources are expected to be strongly globally sub-Gaussian. This is confirmed experimentally in Section 4.

References

[1] J.-F. Cardoso, Blind signal separation: statistical principles, Proceedings of the IEEE 86 (1998) 2009-2025.

[2] A. Cichocki, W. Kasprzak, S.I. Amari, Multi-layer neural networks with a local adaptive learning rule for blind separation of source signals, in: Proc. NOLTA '95, International Symposium on Nonlinear Theory and Its Applications (Las Vegas 1995) 61-65.

[3] N. Delfosse and P. Loubaton, Adaptive blind separation of independent sources: a deflation approach, Signal Processing 45 (1995) 59-84.

[4] P.R.M. Denne and C.D. Hook, Identification systems, UK patent no. 2 157 132 A, published 16 Oct. 1985.

[5] Y. Deville, A unified stability analysis of the Hérault-Jutten source separation neural network, Signal Processing 51 (1996) 229-233.

[6] Y. Deville, Application of the Hérault-Jutten source separation neural network to multi-tag radio-frequency identification systems, in: Proc. Ecole des Techniques Avancées en Signal Image Parole (Grenoble, 1996) 265-272.

[7] Y. Deville, Analysis of the convergence properties of self-normalized source separation neural networks, IEEE Transactions on Signal Processing 47 (1999) 1272-1287.

[8] Y. Deville and N. Charkani, Analysis of the stability of time-domain source separation algorithms for convolutively mixed signals, in: Proc. ICASSP 97, IEEE International Conference on Acoustics, Speech, and Signal Processing (IEEE Press, Munich, 1997) 1835-1838.

[9] Y. Deville and N. Charkani, Convergence of source separation neural networks operating with self-normalized weight updating terms, in: Proc. ICA'99, International Workshop on Independent Component Analysis and Blind Signal Separation (Aussois, France, 1999) 227-232.

[10] S. Drews, W. Tobergte, V. Timm, K. Axer, Verfahren zum Steuern des Zugriffs auf einen Speicher sowie Anordnung zur Durchfuehrung des Verfahrens, German patent no. 4205567.9, European patent no. 0558132, published 26 Aug. 1993.

[11] J.-C. Fort, Stabilité de l'algorithme de séparation de sources de Jutten et Hérault, Traitement du Signal 8 (1991) 35-42.

[12] C.D. Hook, C.S. Hall, Transponder system, European patent no. 0 527 172 B1, published 5 Apr. 1995.

[13] A. Hyvärinen and E. Oja, A fast fixed-point algorithm for independent component analysis, Neural Computation 9 (1997) 1483-1492.

[14] C. Jutten and J. Hérault, Une solution neuromimétique au problème de séparation de sources. Traitement du Signal 5 (1988) 389-403.

[15] C. Jutten and J. Hérault, Blind separation of sources, Part I: An adaptive algorithm based on neuromimetic architecture, Signal Processing 24 (1991) 1-10.

[16] O. Macchi, E. Moreau, Self-adaptive source separation, Part I: convergence analysis of a direct linear network controled by the Hérault-Jutten algorithm IEEE Transactions on Signal Processing 45 (1997) 918-926.

[17] E. Moreau, Apprentissage et adaptativité. Séparation auto-adaptative de sources indépendantes, Ph.D. Thesis, Université Paris XI (Orsay) 1995.

[18] E. Moreau, O. Macchi, Self-adaptive source separation, Part II: comparison of the direct, feedback and mixed linear network, IEEE Transactions on Signal Processing 46 (1998) 39-50.

[19] Philips Semiconductors data sheet, OM 4282 RF-Identification, Hardware description & tutorial, ID-No: 8962D26CEA20068F.

[20] Philips Semiconductors data sheet, OM 4282 RF-Identification, Software command reference & RS 232 transmission protocol, ID-No: 7F3C1206084C995E.

[21] E. Sorouchyari, Blind separation of sources, Part III: Stability analysis, Signal Processing 24 (1991) 21-29.

[22] W. Tobergte, Datenaustauschanordnung, German patent no. 4323530.1, European patent no. 0634729, published 19 Jan. 1995.

Biographies

Yannick Deville was born in Lyon, France, in 1964. He graduated from the Ecole Nationale Supérieure des Télécommunications de Bretagne (Brest, France) in 1986. He received the D.E.A and Ph.D degrees, both in Microelectronics, from the University of Grenoble (France), in 1986 and 1989 respectively. From 1986 to 1997, he was with the Laboratoires d'Electronique Philips at Limeil (France), where he was a Senior Research Scientist. His investigations during this period concerned various fields, including GaAs integrated microwave RC active filters, VLSI cache memory replacement algorithms and architectures, neural network algorithms and applications, and nonlinear systems. Since

1997, he has been a Professor at the University of Toulouse (France). His current major research interests include signal processing, neural networks and especially blind source separation methods and their acoustic and electromagnetic applications.

Jacques Damour has been with the Laboratoires d'Electronique Philips since 1968. Until the end of the '80s, he was involved in the characterization of vacuum tubes designed in these labs. Since the beginning of the '90s, his interests have mainly concerned hardware and software aspects of microcontroller and DSP-based systems, and their use in source separation applications.

Nabil Charkani was born on October 1970. He received the Engineer diploma and DEA degree (both with highest honours) from the Ecole Nationale d'Electronique et de Radioélectricité de Grenoble (INPG - France) in 1993. In 1996, he obtained a Ph.D degree (with highest honours) from INPG completed at Laboratoires d'Electronique of Philips (LEP-Paris) in the area of Source separation and Speech processing. In 1997, he joined Philips Consumer Communications (France), as an R&D engineer in the Advanced Development Department. From early 1998, he was the technical leader of the Digital Signal Processing team and the 'Audio Improvement' project manager. During this period, he initiated and developed numerous projects on speech quality improvement in mobile telephony. Since 2000, he is the manager of the 'Advanced receivers for 3G/3G+' project where he develops new solutions for intra and inter-cell interference cancellation in UMTS and co-ordinates PCC actions in the advanced receivers field. Mr. Charkani is co-author of over 15 papers and inventor of 7 patents for PCC (3 patents are implemented in all Philips mobile phones). He received the 'INPG Best PhD Awards' in Signal Processing in 1997.

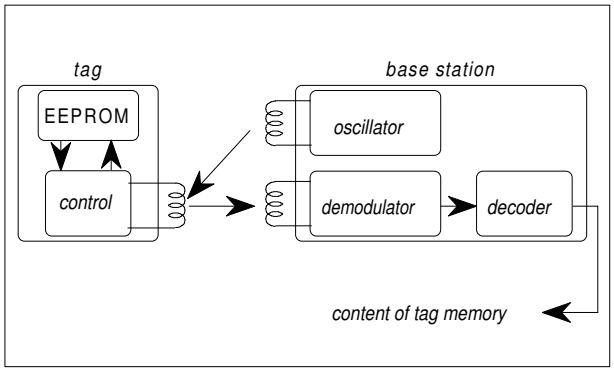

Figure 1: Single-tag RF identification system.

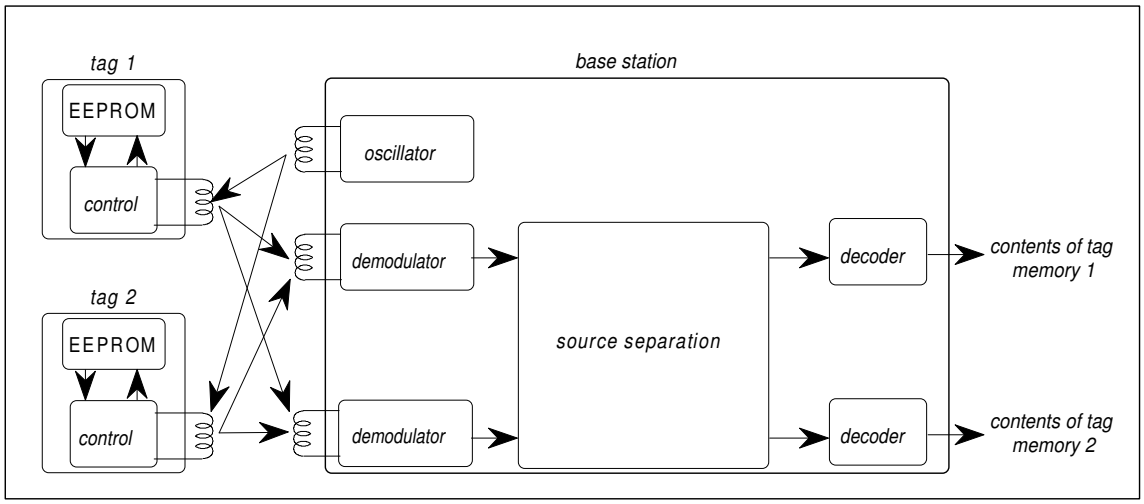

Figure 2: Multi-tag RF identification system.

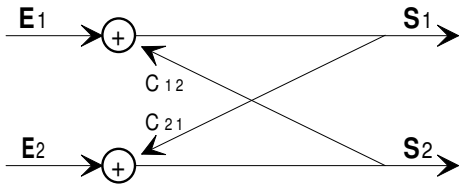

Figure 3: Hérault-Jutten recurrent neural network.

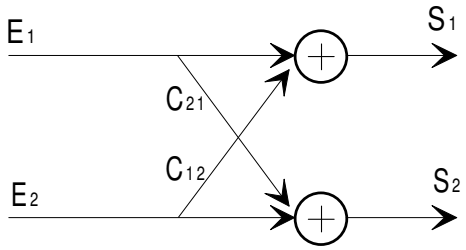

Figure 4: Moreau-Macchi direct neural network.

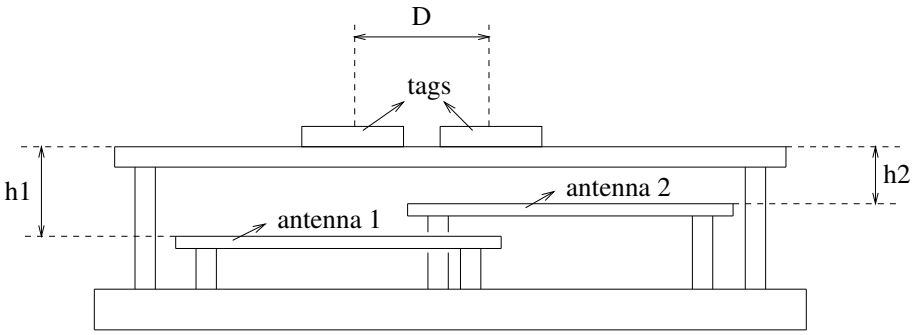

Figure 5: Vertical section of the experimental setup.

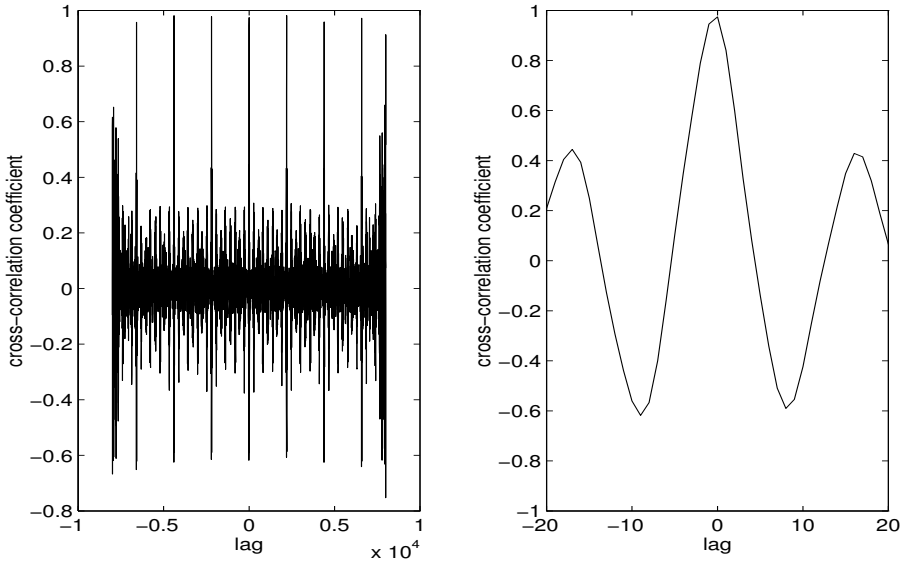

(a) (b)

Figure 6: Sequence of cross-correlation coefficients. (a): complete sequence, (b): zoom around lag zero.

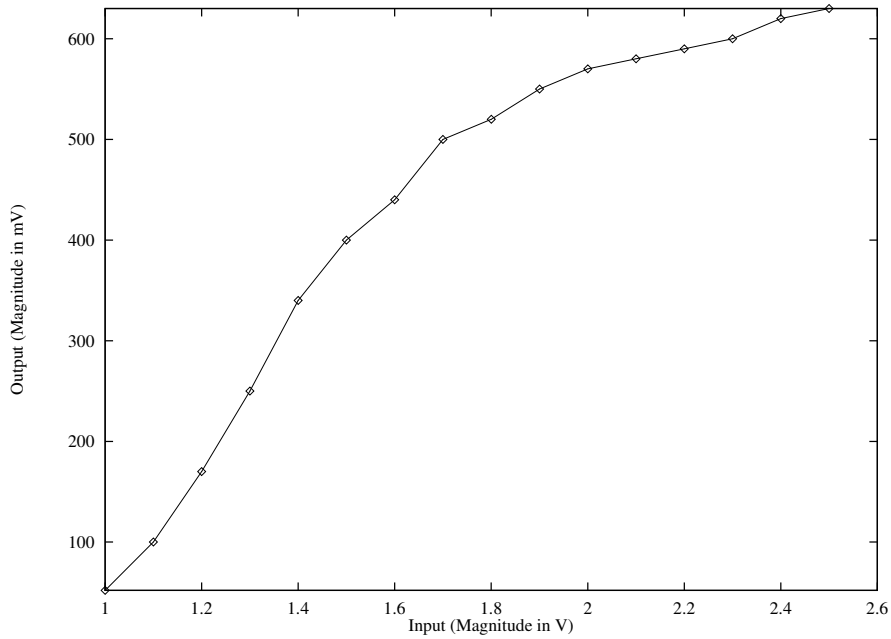

Figure 7: Magnitude of demodulator output vs. magnitude of signal used to modulate input carrier.

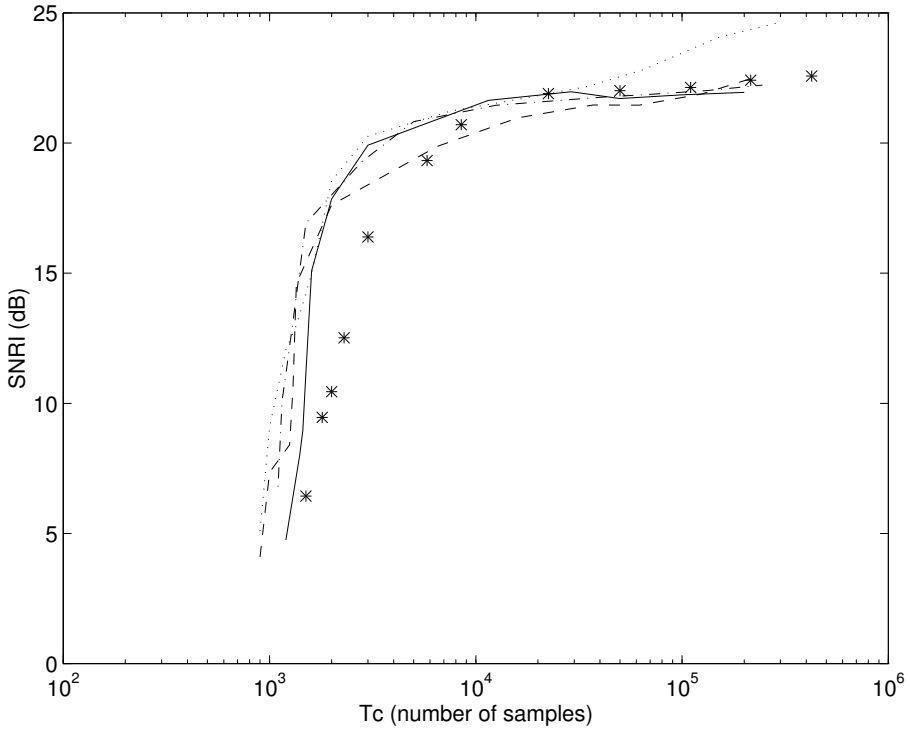

Figure 8: $SNRI$ vs convergence time T_c, when $a_{12} = 0.4$ and $a_{21} = 0.3$. Each plot corresponds to a neural network: Hérault-Jutten: -.-. Moreau-Macchi: .... Cichocki: * * NWUr: — NWUd: - -

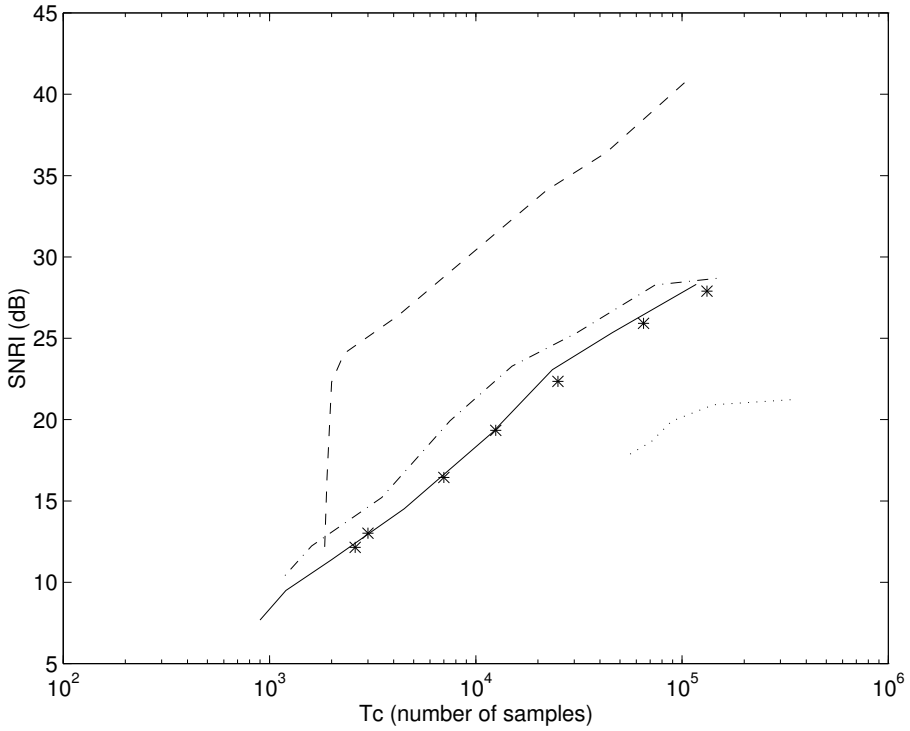

Figure 9: $SNRI$ vs convergence time T_c, when $a_{12} = 0.98$ and $a_{21} = 0.98$. Each plot corresponds to a neural network: Hérault-Jutten: -.-. Moreau-Macchi: .... Cichocki: * * NWUr: — NWUd: - - (for the Moreau-Macchi and Cichocki networks, lower values of T_c than those provided in this figure cannot be reached, as T_c and $SNRI$ then become very sensitive to an increase of the adaptation gain a, and these networks eventually diverge when a is further increased).

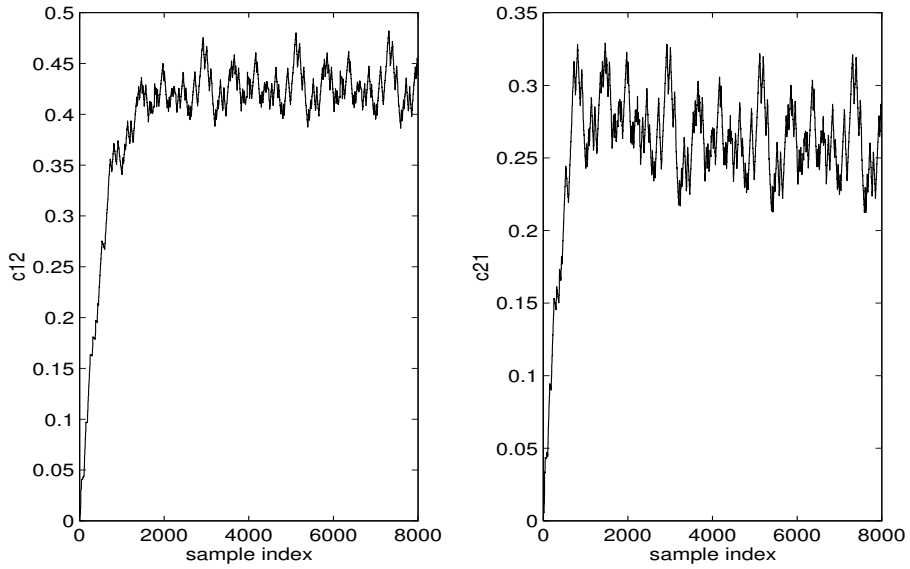

Figure 10: Evolution of the weights of the NWUr network for real mixtures.

Figures captions:

Fig. 1: Single-tag RF identification system.

Fig. 2: Multi-tag RF identification system.

Fig. 3: Hérault-Jutten recurrent neural network.

Fig. 4: Moreau-Macchi direct neural network.

Fig. 5: Vertical section of the experimental setup.

Fig. 6: Sequence of cross-correlation coefficients. (a): complete sequence, (b): zoom around lag zero.

Fig. 7: Magnitude of demodulator output vs. magnitude of signal used to modulate input carrier.

Fig. 8: $SNRI$ vs convergence time T_c, when $a_{12} = 0.4$ and $a_{21} = 0.3$. Each plot corresponds to a neural network: Hérault-Jutten: -.-. Moreau-Macchi: .... Cichocki: * * NWUr: — NWUd: - -

Fig. 9: $SNRI$ vs convergence time T_c, when $a_{12} = 0.98$ and $a_{21} = 0.98$. Each plot corresponds to a neural network: Hérault-Jutten: -.-. Moreau-Macchi: .... Cichocki: * * NWUr: — NWUd: - - (for the Moreau-Macchi and Cichocki networks, lower values of T_c than those provided in this figure cannot be reached, as T_c and $SNRI$ then become very sensitive to an increase of the adaptation gain a, and these networks eventually diverge when a is further increased).

Fig. 10: Evolution of the weights of the NWUr network for real mixtures.